Signal Processing and Renewable Energy
September 2023, (pp. 53-76)
ISSN: 2588-7327
eISSN: 2588-7335

Coordinated Control and Energy Management of Distributed Generation Inverter Using Robust Control in Microgrid

Amin Mavali [1], Ali Naderi Saatlo [1*]

[1] Department of Electrical-Electronics Engineering Urmia Branch, Islamic Azad University, Urmia, Iran.

Received: 20-Feb-2023, Revised: 21-Apr-2023, Accepted: 06-May-2023.

Abstract

A new method to control a micro-grid consisting of various distributed generation (DG) units which are connected to the distribution grid is presented in this paper. In this regard, an energy-management algorithm based on robust control is realized to coordinate the performances of the battery in the micro-grid for grid-connected networks and islanded performances. The designed controller for DG inverters employs a novel algorithm of predictive control which provides faster computation time for high consumer power systems by improving the transient control and steady-state problems, separately. In addition, a micro-grid consisting of a proton-exchange membrane fuel cell (PEMFC), a photovoltaic (PV) array, and a lithium-ion storage battery (SB) is considered. In order to reduce the overall computation time of the system, the designed controller for DG inverters employs a newly developed MPC algorithm which decomposes the control problem into transient sub-problems and steady state. The entire presented system is simulated using MATLAB and then simulation results illustrate the effective performance of the proposed system. Micro-grids with renewable DGs such as solar cells and lithium-ion batteries that are connected to the network via converters are used as the reactive power compensation of nonlinear loads. A robust control method is used for controlling the inverter switches for batteries connected to the power network. An approach based on a robust control study is used in the formation of H_infinity, considering the transient and steady-state response when the system voltage and frequency have priority. Assessments use this method to control voltage and frequency in micro-grid scenarios.

Keywords: Micro-grid, Energy management, Robust control, H_infinity, Frequency control.

1. INTRODUCTION

In recent years, effective application of control and communication methods based on power management systems such as electric vehicles, power grids, and micro-

***Corresponding Authors Email: a.naderi@iaurmia.ac.ir

grids has been proposed [1]–[5]. These study materials involve energy management method in order to balance power on the network, appearing in the real and imaginary components. These trends provide higher levels of penetration of renewable and sustainable generation, such as solar and wind power into the grid. However, these renewable sources are irregular in their generation, therefore they might compromise the stability and reliability of the network [4]–[8]. When a fault occurs in the network components such as actuators, sensors, and plants, it leads to performance degradation and even causes instability of the network. Thus, there is a critical necessity to design fault tolerant controllers (FTCs) to compensate for error effects and guarantee the system's reliability and stability with effective performance.

Generally, the FTCs are categorized into two types: active and passive fault tolerant control. The active fault tolerant control (AFTC) technique usually requires a fault detection and isolation (FDI) scheme which includes a task to detect and localize errors that eventually occur in the network. The passive fault tolerant control (PFTC) is based on robust control techniques which makes the system insensitive to certain faults that are taken into account in the design step. This technique needs no redesign and online detection of errors and therefore is more interesting.

Three-phase induction motors (IMs) are very important in industry because of their reliability, high performance, and low costs [4]. However, due to environmental, mechanical, thermal, and electrical stresses, IMs are addressed to multiple faults. Stator and rotor failures including eccentricity and broken bars are the most famous asymmetric faults. The eccentricity faults can be categorized into two types: static eccentricity and dynamic eccentricity. The static and dynamic eccentricities can cause stator and rotor asymmetries, respectively [5-6].

From AFTC point of view, different FDI techniques have been proposed for IM. In [7-9], the authors have detected the broken bar fault by model-based parameter estimation techniques. Multiple signal processing techniques such as fast Fourier transform (FFT) are studied in [10-11]. In [12-14], artificial intelligence techniques have been discussed for fault detection. Furthermore, some other sliding modes [15], adaptive [16], and sensorless methods [17-21] have been proposed in recent years.

From PFTC point of view, the sliding mode control (SMC) technique has received great attention due to its robust behavior against model uncertainties [22]. In [23], the authors have proposed an approach which detects the occurrence of a fault and switches itself between a nominal operation controller and a sliding mode faulty controller. In [24], a second-order sliding mode controller (SOSMC) has been designed based on the backstepping method. The SOSMC is utilized to avoid the chattering phenomenon; moreover, the backstepping method is applied to bring the IM model nonlinearities into the control inputs direction. However, both of the mentioned pieces of literature only have studied the rotor broken bar fault and there is no attention to other faults like the stator eccentricity.

In this paper, two fault-tolerant sliding mode controllers are developed for IM in

order to attenuate the effects of the stator and rotor faults (broken bar and eccentricity) and the load torque variations. The first controller is developed based on the NBC technique which has been reported in [25-26]. This NBC technique is a powerful tool to handle nonlinearities of the IM model. However, it is computationally burden and it is not able to remove the complete effects of non-vanishing unmatched faults/uncertainties. To solve the mentioned problem, an improved NBC technique is proposed, which is the first novelty of this study. On the other hand, since the SMC with a linear sliding surface presents slow transient responses and considerable tracking errors [27], a novel nonlinear sliding surface is suggested that shows a fast transient response with small tracking errors. This technique is known as nonlinear sliding mode control (NSMC).

The paper is organized as follows: In Section 2, the IM healthy and faulty dynamical models are presented. Two NBC transformation techniques are implemented for IM faulty model in Section 3. In Section 4, two robust fault-tolerant sliding mode controllers are developed based on the NBC transformated models. In section 5, the merits of the designed controllers are verified by the simulations on IM subjected to the matched/unmatched faults and load torque disturbances. Finally, conclusions are given in Section 6.

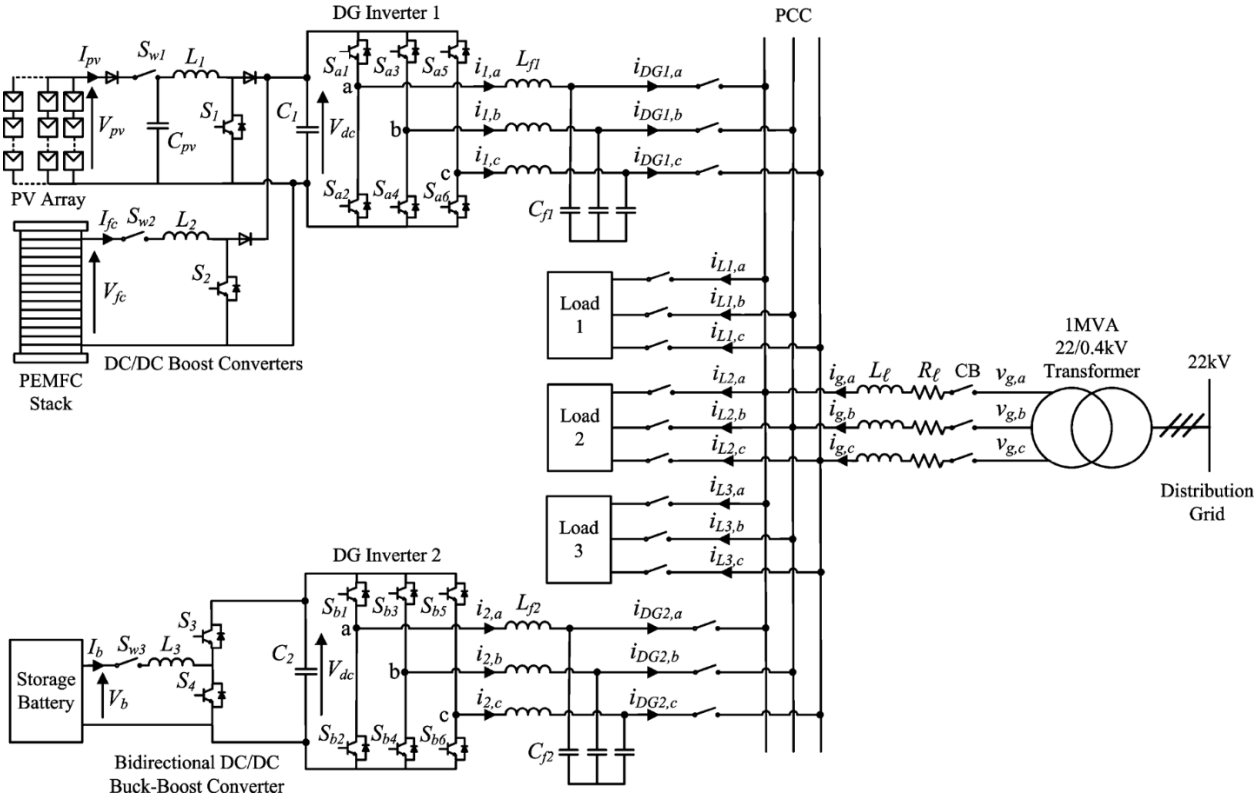

Fig. 1. Configuration of proposed micro-grid.

2. STUDIED MODELS OF MICRO-GRID

Figure 1 shows the micro-grid structure studied in this paper. According to the figure, the micro-grid can be connected to the network or be considered as an islanded micro-grid. The main DG unit includes a 15-kW PEMFC and 40-kW PV array, which have been connected in the parallel form to the DC side of DG inverter 1 by a DC/DC boost converter in order to regulate the DC-link voltage of the DG inverter in an optimum level by delivering the required power. In this configuration, the PEMFC is employed to support the intermittent generation of the PV array, and the PV array is realized in the form of a primary generation unit. In the case that there is large sunlight, the PV array acts in the MPPT state in order to provide maximum DC power. Under balance operation, the state space model of an inverter is presented in the synchronously rotating reference frame (d-q) according to the following equations [23-24, 28]:

$$
\begin{aligned}
&v_{ds} = R_s i_{ds} + \frac{d\psi_{ds}}{dt} - \omega_s \psi_{qs} \\
&v_{qs} = R_s i_{qs} + \frac{d\psi_{qs}}{dt} + \omega_s \psi_{ds} \\
&v_{dr} = 0 = R_r i_{dr} + \frac{d\psi_{dr}}{dt} - (\omega_s - \omega_r)\psi_{qr} \\
&v_{qr} = 0 = R_r i_{qr} + \frac{d\psi_{qr}}{dt} + (\omega_s - \omega_r)\psi_{dr} \\
&\psi_{ds} = L_s i_{ds} + L_m i_{dr}, \quad \psi_{qs} = L_s i_{qs} + L_m i_{qr} \\
&\psi_{dr} = L_r i_{dr} + L_m i_{ds}, \quad \psi_{qr} = L_r i_{qr} + L_m i_{qs} \\
&\frac{d\omega_m}{dt} = \frac{1}{J}\left(T_e - F\omega_m - T_L\right), \qquad \omega_r = p\omega_m \\
&T_e = p\frac{L_m}{L_r}\left(\psi_{dr} i_{qs} - \psi_{qr} i_{ds}\right)
\end{aligned}
\tag{1}
$$

where i_{ds}, i_{qs} are the components of the stator current, ψ_{dr}, ψ_{qr} are the components of the rotor flux, v_{ds}, v_{qs} are the stator voltage components, v_{dr}, v_{qr} are the rotor voltage components, ω_s is the stator pulsation, ω_r is the electrical angular speed, ω_m is the mechanical speed, R_s and R_r are stator and rotor resistances, L_s and L_r are stator and rotor inductances and L_m is the mutual inductance, p is the number of pole pairs, T_e is the electromagnetic torque, T_L is an unknown load torque, J is the moment of inertia coefficient, and F is the friction coefficient.

Based on the FOC strategy, the coupling between the rotor flux vector $[\psi_{dr}, \psi_{qr}]^T$ and the electromagnetic torque T_e should be reduced. This coupling is reducible by selecting the rotor flux orientation as follows [23-24]:

$$
\psi_{dr} = \psi_r \quad , \psi_{qr} = 0 \tag{2}
$$

From the above assumption, the inverter model will be simplified as:

$$
\begin{aligned}
&\frac{d\omega_m}{dt} = \frac{pL_m}{L_r J} i_{qs}\psi_{dr} - \frac{F}{J} - \frac{T_L}{J} \\
&\frac{d\psi_{dr}}{dt} = \frac{L_m}{\tau_r} i_{ds} - \frac{1}{\tau_r}\psi_{dr} \\
&\frac{di_{ds}}{dt} = -a i_{ds} + \omega_s i_{qs} + \frac{L_m}{\sigma L_s L_r \tau_r}\psi_{dr} + \frac{v_{ds}}{\sigma L_s} \\
&\frac{di_{qs}}{dt} = -a i_{qs} - \omega_s i_{ds} - \frac{L_m P p}{\sigma L_s L_r}\omega_m \psi_{dr} + \frac{v_{qs}}{\sigma L_s}
\end{aligned}
\tag{3}
$$

with

$$\omega_s = p\omega_m + \frac{L_m}{\tau_r \psi_{dr}} i_{qs} \quad (4)$$

where $\tau_r = \frac{L_r}{R_r}$ is the rotor time constant, $\sigma = 1 - \frac{L_m^2}{L_s L_r}$ is the coefficient of dispersion, and $a = \left(\frac{R_s}{\sigma L_s} + \frac{1-\sigma}{\sigma \tau_r} \right)$ is a constant.

2.1. IM Faulty Model

In this study, two classes of faults in the IM model are considered [5-6]:

1- Rotor asymmetries, which accrue because of dynamic eccentricity or broken rotor bars; Broken rotor bars lead to the variation of rotor resistance. This variation can be modeled by substituting $R_r + \Delta R_r$ instead of R_r into the IM dynamic model (3).

2- Stator asymmetries, because of static eccentricity. According to literature [6], in the presence of dynamic and static eccentricities, it causes asymmetries in the induction motor which is generated due to faults which in turn yields some slot harmonics in the stator winding. This effect can be modeled by considering a sinusoidal fault term to the stator present values. Especially, letting $i_d^{uf}(t)$ and $i_q^{uf}(t)$ indicate the stator present values without any faults. Also $i_d^f(t)$ and $i_q^f(t)$ are the same values while faults exist. Take notice that this current can be explained as:

$$\begin{aligned} i_{sd}^f(t) &= i_{sd}^{uf} + A\sin(\omega_c(t) + \theta_s(t) + \varphi), \\ i_{sq}^f(t) &= i_{sq}^{uf} + A\cos(\omega_c(t) + \theta_s(t) + \varphi) \end{aligned} \quad (5)$$

where the phase φ and the amplitude A are unknown and depend on the stator or rotor faults entity.

If we suppose that faults just happen when the induction motor works in a steady operation, then:

$$\begin{aligned} \omega_c(t) + \theta_s(t) &= 2\pi ft \\ &\quad + (p\omega_{m,ref} + \omega_{sl})t + \theta_{s0} \end{aligned} \quad (6)$$

In faults, the dynamic eccentricity is concerned, therefore:

$$\begin{aligned} \omega_c(t) + \theta_s(t) &= 2(\pi f \pm 2k\omega_{sl})t \\ &\quad + (p\omega_{m,ref} + \omega_{sl})t + \theta_{s0} \end{aligned} \quad (7)$$

where $\omega_{sl} = \omega_s - p\omega_{m,ref}$ is the slip angular frequency, $\omega_{m,ref}$ is the reference of rotor speed, f is the supply frequency, θ_{s0} denotes the unknown position of reference frame when the fault exists, $k = 1,....N$ is the finite integer.

From the above-mentioned faults, the IM faulty model can be described as:

$$\begin{aligned} \frac{d\omega_m}{dt} &= \frac{pL_m}{L_r J} i_{qs}\psi_{dr} - \frac{F}{J} + h_1(t) \\ \frac{d\psi_{dr}}{dt} &= \frac{L_m}{\tau_r} i_{ds} - \frac{1}{\tau_r}\psi_{dr} + h_2(t) \\ \frac{di_{ds}}{dt} &= -ai_{ds} + \omega_s i_{qs} + \frac{L_m}{\sigma L_s L_r \tau_r}\psi_{dr} \\ &\quad + \frac{v_{ds}}{\sigma L_s} + h_3(t) \\ \frac{di_{qs}}{dt} &= -ai_{qs} - \omega_s i_{ds} - \frac{L_m Pp}{\sigma L_s L_r}\omega_m \psi_{dr} \\ &\quad + \frac{v_{qs}}{\sigma L_s} + h_4(t) \end{aligned} \quad (8)$$

where $h_1(t) = -\frac{T_L}{J} + h_1(\Delta i_{sdq})$, $h_2(t) =$, $h_2(\Delta i_{sdq}, \Delta R_r)$, $h_3(t) = h_3(\Delta i_{sdq}, \Delta R_r)$ and $h_4(t) = h_4(\Delta i_{sdq}, \Delta R_r)$ depict the fault and uncertainty terms which originate from the variation of rotor resistance, harmonics in the stator winding ($\Delta i_{sdq} = i_{sdq}^{f} - i_{sdq}^{uf}$), and load torque variation. It is worthy to note that the load torque T_L is added with the fault terms due to its typically uncertain nature.

The control objective is to design sliding mode controllers for governing the rotor mechanical speed ω_m and the rotor flux $\psi_r = [\psi_{dr}, \psi_{qr}]^T$ in the presence of faults and uncertainties. By taking a glance at the IM faulty model (8), it is evident that the model is not in the companion form. Therefore, the SMC technique is not applicable directly. To solve this problem, the NBC transformation technique will be developed in the next section.

3. NBC TRANSFORMATION APPLICATION ON IM DYNAMICS

In this section, two types of NBC transformation techniques are expressed. The first one is the conventional NBC technique which is presented in [25-26]. However, because of the elimination of uncertainty problem and reduction in the amount of computation, we have proposed a second approach. More details are presented below:

To make the IM faulty notations (8) less complex, consider the following new variables:

$$\begin{aligned} x_{11} &= \omega_m, \quad x_{12} = \psi_{dr}, \\ x_{21} &= i_{ds}, \quad x_{22} = i_{qs} \end{aligned} \tag{9}$$

Hence, the motor dynamics can be written as:

$$\begin{aligned} \frac{d}{dt}x_{11} &= \frac{pL_m}{L_r J}x_{12}x_{22} - \frac{F}{J}x_{11} + h_1(t) \\ \frac{d}{dt}x_{12} &= \frac{L_m}{\tau_r}x_{21} - \frac{1}{\tau_r}x_{12} + h_2(t) \\ \frac{d}{dt}x_{21} &= -ax_{21} + \omega_s x_{22} + \frac{L_m}{\sigma L_s L_r \tau_r}x_{12} \\ &\quad + \frac{1}{\sigma L_s}v_{ds} + h_3(t) \\ \frac{d}{dt}x_{22} &= -ax_{22} - \omega_s x_{21} - \frac{L_m Pp}{\sigma L_s L_r}x_{11}x_{12} \\ &\quad + \frac{1}{\sigma L_s}v_{qs} + h_4(t) \end{aligned} \tag{10}$$

The system model (10), can be represented in the following NBC-form as:

$$\begin{aligned} \dot{X}_1 &= f_1(X_1) + B_1(X_1)X_2 + H_1(t) \\ \dot{X}_2 &= f_2(X_1, X_2) + B_2 u(t) + H_2(t) \end{aligned} \tag{11}$$

where:

$$X_1 = \begin{bmatrix} x_{11} \\ x_{12} \end{bmatrix}, \quad f_1(X_1) = \begin{bmatrix} -\frac{F}{J}x_{11} \\ -\frac{1}{\tau_r}x_{12} \end{bmatrix}, \quad B_1(X_1) = \begin{bmatrix} 0 & \frac{pL_m}{L_r}x_{12} \\ \frac{L_m}{\tau_r} & 0 \end{bmatrix}, \quad H_1(t) = \begin{bmatrix} h_1(t) \\ h_2(t) \end{bmatrix}$$

$$X_2=\begin{bmatrix} x_{21} \\ x_{22} \end{bmatrix}, \qquad f_2(X_1,X_2)=\begin{bmatrix} -ax_{21}+\omega_s x_{22}+\dfrac{L_m}{\sigma L_s L_r \tau_r}x_{12} \\ -ax_{22}-\omega_s x_{21}-\dfrac{L_m p}{\sigma L_s L_r}x_{11}x_{12} \end{bmatrix}, \qquad B_2=\begin{bmatrix} \dfrac{1}{\sigma L_s} & 0 \\ 0 & \dfrac{1}{\sigma L_s} \end{bmatrix}$$

$$u(t)=\begin{bmatrix} v_{ds} \\ v_{qs} \end{bmatrix}, \qquad H_2=\begin{bmatrix} h_3(t) \\ h_4(t) \end{bmatrix}$$

The NBC-form (11) is composed of two blocks, where X_2 is the fictitious control for the first block, and $H_1(t)$ and $H_2(t)$ are the unmatched and matched fault vectors, respectively.

Assumption 1: Assume that the fault vectors be bounded as:

$$\|H_1(t)\| < H_{1\max} \tag{12}$$

$$\|H_2(t)\| < H_{2\max} \tag{13}$$

where $H_{1\max}$ and $H_{2\max}$ are known positive constants.

3.1. Conventional NBC

Now, let us define the following tracking errors:

$$\begin{aligned} Z_1 &= \begin{bmatrix} z_{11} \\ z_{12} \end{bmatrix} = X_{1,ref} - X_1 \\ &= \begin{bmatrix} x_{11,ref}-x_{11} \\ x_{12,ref}-x_{12} \end{bmatrix} = \begin{bmatrix} \omega_{m,ref}-\omega_m \\ \psi_{dr,ref}-\psi_{dr} \end{bmatrix} \end{aligned} \tag{14}$$

where $X_{1,ref}$ is the desired value of X_1. The time derivative of (14) is:

$$\dot{Z}_1 = \dot{X}_{1,ref} - \dot{X}_1 \tag{15}$$

Substituting the first block of (11) in (15), yields:

$$\begin{aligned} \dot{Z}_1 = &- f_1(X_1) + \dot{X}_{1,ref} \\ &- B_1(X_1)X_2 - H_1(t) \end{aligned} \tag{16}$$

Let the fictitious control input X_2 for (16) be chosen as:

$$\begin{aligned} X_2 = &B_1^{-1}(X_1) \\ &[-f_1(X_1) + \dot{X}_{1,ref} + K_1 Z_1 - Z_2] \end{aligned} \tag{17}$$

where Z_2 is a new variable, and $K_1=\begin{bmatrix} k_{11} & 0 \\ 0 & k_{12} \end{bmatrix}$, $k_{11}>0$, $k_{12}>0$ is the control gain matrix. Inserting the virtual control law (17) into (16) results in the first transformation block in the new coordinates:

$$\dot{Z}_1 = -K_1 Z_1 + Z_2 - H_1(t) \tag{18}$$

From (17), Z_2 can be derived as follows:

$$\begin{aligned} Z_2 = &f_1(X_1) - \dot{X}_{1,ref} - K_1 Z_1 \\ &+ B_1(X_1)X_2 \end{aligned} \tag{19}$$

The time derivative of (19) is:

$$\begin{aligned} \dot{Z}_2 = &\frac{d}{dt}(f_1(X_1)) - \ddot{X}_{1,ref} - K_1 \dot{Z}_1 \\ &+ \frac{d}{dt}\big(B_1(X_1)\big)X_2 + B_1(X_1)\dot{X}_2 \end{aligned} \tag{20}$$

The above equation can be represented as:

$$\dot{Z}_2 = F(Z_1, Z_2, X_1, X_{1,ref}, X_2) + B(X_1)u(t) + H(t) \quad (21)$$

with the following details:

$$F(Z_1, Z_2, X_1, X_{1,ref}, X_2) = \begin{bmatrix} -\frac{F}{J} & 0 \\ 0 & -\frac{1}{\tau_r} \end{bmatrix} (K_1 Z_1 - Z_2 + \dot{X}_{1,ref}) - \ddot{X}_{1,ref} - K_1(-K_1 Z_1 + Z_2)$$

$$+ \begin{bmatrix} 0 & \frac{pL_m}{L_r J}(k_{12} z_{12} - z_{22} + \dot{x}_{12,ref}) \\ 0 & 0 \end{bmatrix} X_2 + B_1(X_1) f_2(X_1, X_2)$$

$$B(X_1) = B_1(X_1) B_2$$

$$H(t) = \left(K_1 + \begin{bmatrix} -\frac{F}{J} & 0 \\ 0 & -\frac{1}{\tau_r} \end{bmatrix} \right) H_1(t) + B_1(X_1) H_2(t) + \begin{bmatrix} \frac{pL_m}{L_r J} \\ 0 \end{bmatrix} h_{12}$$

From (18) and (21), the IM first transformed model can be expressed in the new coordinates (Z_1, Z_2) as follows:

$$\begin{aligned} \dot{Z}_1 &= -K_1 Z_1 + Z_2 - H_1(t) \\ \dot{Z}_2 &= F(Z_1, Z_2, X_1, X_{1,ref}, X_2) \\ &\quad + B(Z_1, X_{1,ref})u(t) + H(t) \end{aligned} \quad (22)$$

Remark 1: The above transformation model contains three main drawbacks:

1- Deriving the second block dynamic is troublesome due to the lengthy computation of (20).

For high-dimensional systems, this problem will be a real challenge and needs to be solved.

2- In designing controllers, low tracking error ($Z_1 \to 0$) is hard to achieve due to the non-vanishing uncertainties like T_L in the unmatched vector $H_1(t)$. To avoid this problem, the load torque T_L should be known by measuring or approximating it.

3- There is no reference value for X_2. In the other word, governing the virtual state X_2 is not considered so important, and this inconsideration case causes some problems in practical applications.

The next transformation technique is able to improve the mentioned problems.

3.2. Improved NBC

Consider the following tracking errors:

$$\begin{aligned} Z_1 &= X_{1,ref} - X_1 = \begin{bmatrix} z_{11} \\ z_{12} \end{bmatrix} \\ &= \begin{bmatrix} x_{11,ref} - x_{11} \\ x_{12,ref} - x_{12} \end{bmatrix} = \begin{bmatrix} \omega_{m,ref} - \omega_m \\ \psi_{dr,ref} - \psi_{dr} \end{bmatrix} \\ Z_2 &= X_{2,ref} - X_2 = \begin{bmatrix} z_{21} \\ z_{22} \end{bmatrix} \\ &= \begin{bmatrix} x_{21,ref} - x_{21} \\ x_{22,ref} - x_{22} \end{bmatrix} = \begin{bmatrix} i_{ds,ref} - i_{ds} \\ i_{qs,ref} - i_{qs} \end{bmatrix} \end{aligned} \quad (23)$$

Taking the time derivative of Z_1 and substituting the first block of (11) in it, yields:

$$\begin{aligned}\dot{Z}_1 &= \dot{X}_{1,ref} - \dot{X}_1 \\ &= \dot{X}_{1,ref} - f_1(X_1) \\ &\quad - B_1(X_1)(X_{2,ref} - Z_2) - H_1(t) \\ &= -f_1(X_1) + \dot{X}_{1,ref} - B_1(X_1)X_{2,ref} \\ &\quad + B_1(X_1)Z_2 - H_1(t)\end{aligned} \tag{24}$$

In (24), we replaced X_2 by $X_{2,ref} - Z_2$. Hence, $X_{2,ref}$ will be the fictitious control input instead of X_2. This replacement is the main reason for the derivational calculation reduction.

Now, let's propose the fictitious control input $X_{2,ref}$ for (24) as:

$$\begin{aligned}X_{2,ref} = B_1^{-1}(X_1)\big(&-f_1(X_1) + \dot{X}_{1,ref} \\ &+ K_1 Z_1 + K_{sw1}\tanh(Z_1/\rho_1)\big)\end{aligned} \tag{25}$$

where $\tanh(\cdot)$ is the hyperbolic tangent function and is the approximation of $\mathrm{sgn}(\cdot)$, ρ_1 is a small enough positive constant, and $K_{sw1} = \begin{bmatrix} k_{sw11} & 0 \\ 0 & k_{sw12} \end{bmatrix}$ is the sliding gain and that should be selected in such a way that $\|K_{sw1}\| > H_{1\max}$.

By substituting the virtual control law (25) into (24), we have:

$$\begin{aligned}\dot{Z}_1 &= -K_1 Z_1 + B_1(X_1)Z_2 \\ &\quad - K_{sw1}\tanh(Z_1/\rho_1) - H_1(t)\end{aligned} \tag{26}$$

Moreover, calculating the time derivative of Z_2 and inserting the second block of (11) into it, yields:

$$\begin{aligned}\dot{Z}_2 &= \dot{X}_{2,ref} - \dot{X}_2 = -f_2(X_1, X_2) \\ &\quad + \dot{X}_{2,ref} - B_2 u(t) - H_2(t)\end{aligned} \tag{27}$$

From (26) and (27), the IM second transformation model can be expressed in the new coordinates (Z_1, Z_2) as follows:

$$\begin{aligned}\dot{Z}_1 &= -K_1 Z_1 + B_1(X_1)Z_2 \\ &\quad - K_{sw1}\tanh(Z_1/\rho_1) - H_1(t) \\ \dot{Z}_2 &= -f_2(X_1, X_2) + \dot{X}_{2,ref} \\ &\quad - B_2 u(t) - H_2(t)\end{aligned} \tag{28}$$

It is worthy noting that compared to the conventional NBC:

1- The second block dynamic (27) is determined easily with no more derivational calculations.

2- The non-vanishing unmatched fault and uncertainty effects can be attenuated by the robust term $K_{sw1}\tanh(Z_1/\rho_1)$.

3- Converging $Z_2 \to 0$, will result in $X_2 \to X_{2,ref}$.

4. FAULT TOLERANT SLIDING MODE CONTROL

In this section, two fault tolerant sliding mode controllers are designed for the conventional and the improved NBC transformation models.

4.1. SMC with the Conventional NBC

Let us define the following sliding manifold:

$$s(t) = Z_2(t) = 0 \tag{29}$$

By taking the time derivative from (29) and using (22), we can obtain:

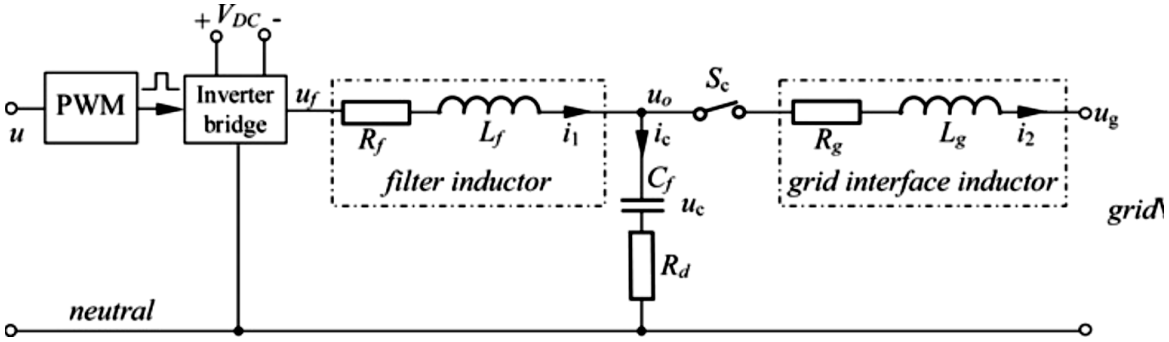

Fig. 2. Single phase schematic of inverter combined by filter.

$$\dot{s}(t) = F(Z_1, Z_2, X_1, X_{1,ref}, X_2) + B(X_1)u(t) + H(t) \tag{30}$$

Theorem 1: Consider the IM first transformed NBC model (22) with the linear sliding surface (29) and Assumption 1, then the following control law is considered:

$$u(t) = B^{-1}(X_1)[-F(Z_1, Z_2, X_1, X_{1,ref}, X_2) - K_2 Z_2 - K_{sw2}\,\mathrm{sgn}(s(t))] \tag{31}$$

which guarantees zero convergence of Z_2, and boundedness of Z_1 around zero. Hence, the IM speed and flux tracking errors convergence around the origin will be assured. Where

$K_2 = \begin{bmatrix} k_{21} & 0 \\ 0 & k_{22} \end{bmatrix}$, $k_{21} > 0$, $k_{22} > 0$,

$K_{sw2} = \begin{bmatrix} k_{sw21} & 0 \\ 0 & k_{sw22} \end{bmatrix}$, and

$K_{sw} > H_{\max} > \|H(t)\|$.

Stability proof: In order to assure the closed-loop system stability, consider the following Lyapunov candidate:

$$V = \frac{1}{2} s_2^T s_2 \tag{32}$$

Taking time derivative from (32) and using (30) and (31), result in:

$$\begin{aligned} \dot{V} &= s_2^T \dot{s}_2 = Z_2^T \dot{Z}_2 \\ &= Z_2^T (F(Z_1, Z_2, X_1, X_{1,ref}, X_2) \\ &\quad + B(X_1)u(t) + H(t)) \\ &= Z_2^T (-K_2 Z_2 - K_{sw2}\,\mathrm{sgn}(Z_2) \\ &\quad + H(t)) \\ &= -K_2 Z_2^T Z_2 + Z_2^T \left(-K_{sw2}\,\mathrm{sgn}(Z_2) \right. \\ &\quad \left. + H(t)\right) \end{aligned} \tag{33}$$

Selecting $K_{sw} > H_{\max}$ yields:

$$\dot{V} = -K_2 Z_2^T Z_2 < 0 \tag{34}$$

which fulfills $Z_2 \to 0$. Then, the first transformation model (22) can be reduced as:

$$\dot{Z}_1 = -K_1 Z_1 + 0 - H_1(t) \tag{35}$$

From (35), it is obvious that Z_1 will converge to zero for vanishing uncertainties, while $H_1(t)$ has the non-vanishing term T_L in $h_1(t)$. Therefore, the flux convergence is possible ($\psi_{dr} \to \psi_{dr,ref}$), but the mechanical speed will have deviations from the reference speed ($\omega_{m,ref} - \omega_m \to \varepsilon \neq 0$).

It is worthy to note that choosing large values of K_1 can reduce the speed tracking error, but it is not able to remove the error permanently.

4.2. NSMC with the Improved NBC

In this section, the NSMC is applied for the second transformed NBC model (28). In other words, a nonlinear sliding surface is proposed to improve the conventional SMC slow responses.

Consider the following nonlinear sliding manifold:

$$s(t) = Z_2(t) + c\int_0^t Z_2^{\mu}(\tau)d\tau \tag{36}$$

where $s(t) = \left[s_1(t),\ \ s_2(t)\right]^T$, $0 < \mu = \frac{p}{q} < 1$, and p, q are rational odd numbers; in addition, c is a positive constant.

Taking time derivative from (36) yields:

$$\dot{s}(t) = \dot{Z}_2 + cZ_2^{\mu} \tag{37}$$

Inserting (28) into (37) results in:

$$\begin{aligned}\dot{s}(t) = &- f_2(X_1, X_2) + \dot{X}_{2,ref} \\ &+ cZ_2^{\mu} - B_2u(t) - H_2(t)\end{aligned} \tag{38}$$

Theorem 2: Consider the IM second transformed NBC model (28) with the nonlinear sliding surface (36) and Assumption 1, then consider the following control law:

$$\begin{aligned}u(t) = B_2^{-1}\big(&- f_2(X_1, X_2) + \dot{X}_{2,ref} + cZ_2^{\mu} \\ &+ K_2 s(t) + K_{sw2}\,\mathrm{sgn}(s(t))\big)\end{aligned} \tag{39}$$

which guarantees Z_1 and Z_2 zero convergence. Hence, the IM speed and flux tracking errors convergence is assured, where $K_2 = \begin{bmatrix} k_{21} & 0 \\ 0 & k_{22} \end{bmatrix}$, and $\|K_{sw2}\| > H_{2\max}$.

Stability analysis: Let us define the following Lyapunov function:

$$V(t) = 0.5s^T(t)s(t) \tag{40}$$

Taking time derivative from (40) and using (38) and (39), we can get:

$$\begin{aligned}\dot{V}(t) &= s^T(t)\dot{s}(t) \\ \dot{V}(t) &= s^T(t)\big(- f_2(X_1, X_2) + \dot{X}_{2,ref} \\ &\qquad + cZ_2^{\mu} - B_2u(t) - H_2(t)\big) \\ \dot{V}(t) &= s^T(t)\big(-K_2 s(t) \\ &\qquad - K_{sw2}\,\mathrm{sgn}(s(t)) - H_2(t)\big) \\ \dot{V}(t) &= -s^T(t)K_2 s(t) + s^T(t) \\ &\qquad \big(-K_{sw2}\,\mathrm{sgn}(s(t)) - H_2(t)\big)\end{aligned} \tag{41}$$

Selecting $\|K_{sw2}\| > H_{2\max}$ yields:

$$\dot{V}(t) = -s^T(t)K_2 s(t) < 0 \tag{42}$$

which guarantees the second block state vector zero convergence ($Z_2 \to 0$). Then, the equation (28) can be rewritten as:

$$\begin{aligned}\dot{Z}_1 = &-K_1 Z_1 + 0 \\ &- K_{sw1}\tanh(Z_1/\rho_1) - H_1(t)\end{aligned} \tag{43}$$

To analyze (43) stability, consider the following Lyapunov function:

$$V_1(t) = 0.5Z_1^T Z_1 \tag{44}$$

Calculating the time derivative of (44) and substituting (43) into it results in:

$$\begin{aligned}\dot{V}_1(t) &= Z_1^T \dot{Z}_1 = Z_1^T \left(-K_1 Z_1 \right. \\ &\quad \left. - K_{sw1} \tanh(Z_1 / \rho_1) - H_1(t)\right) \\ &= -Z_1^T K_1 Z_1 \\ &\quad + Z_1^T \left(-K_{sw1} \tanh(Z_1 / \rho_1) \right. \\ &\quad \left. - H_1(t)\right)\end{aligned} \tag{45}$$

By selecting the sliding gain $\|K_{sw1}\| > H_{1\max}$, we have:

$$\dot{V}_1(t) = -Z_1^T K_1 Z_1 < 0 \tag{46}$$

which assures $Z_1 \to 0$. The inequality (46) is the main advantage of the second transformation form (28) and the control law (39) over the first transformation form (22) with the control law (31).

5. DESIGN OF ROBUST INVERTER CONTROL BASED ON THE H-INFINITY METHOD

Figure 2 demonstrates the plant model which is obtained via the system single phase diagram. The circuit breaker SC is required during the shutdown and synchronization mechanism.

The currents of the two inductors and the voltage of the capacitor are chosen as state variables of this plant, so we have:

$$x = [i_1 \;\; i_2 \;\; u_c]^T \tag{47}$$

The external input $w = [u_g \;\; u_{ref}]^T$ includes the grid side voltage u_g and the reference voltage that may be tracked is u_{ref}, and finally, the control input of the system is u. The plant state space description can be represented by:

$$\dot{X} = AX + B_1 w + B_2 u \tag{48}$$

Then, the output equation will be:

$$y = e = C_1 x + D_1 w + D_2 u \tag{49}$$

By considering the filter and grid together, we can show:

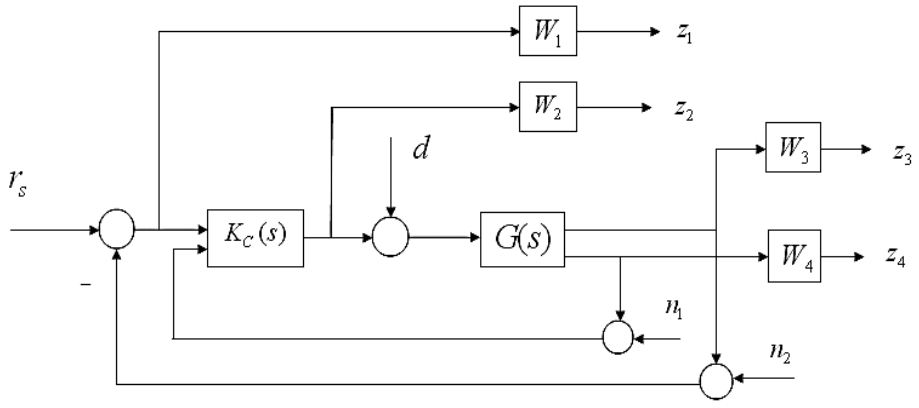

Fig. 3. Representation of robust controller.

$$A=\begin{bmatrix} -\frac{R_f+R_d}{L_f} & \frac{R_d}{L_f} & -\frac{1}{L_f} \\ \frac{R_d}{L_g} & -\frac{R_g+R_d}{L_g} & \frac{1}{L_g} \\ \frac{1}{C_f} & -\frac{1}{C_f} & 0 \end{bmatrix},$$

$$B_1=\begin{bmatrix} 0 & 0 \\ -\frac{1}{L_g} & 0 \\ 0 & 0 \end{bmatrix},\ B_2=\begin{bmatrix} \frac{1}{L_f} \\ 0 \\ 0 \end{bmatrix}, \qquad (50)$$

$$C_1=\begin{bmatrix} -R_d & R_d & -1 \end{bmatrix},\ D_1=\begin{bmatrix} 0 & 1 \end{bmatrix},\ D_2=0$$

In this section, we intend to design a controller inverter system. For this purpose, by taking into account the disturbance input, reference input noise measurements and weights as well as the design, consider the models of figure 2, where the H-infinity technique is employed to design the robust controller which is called $K_C(s)$.

6. SIMULATION RESULTS

This section evaluates the designed robust controller efficiency through extensive simulations using MATLAB / Simulink; the simulation results prove their advantages in comparison with the conventional inverter controller.

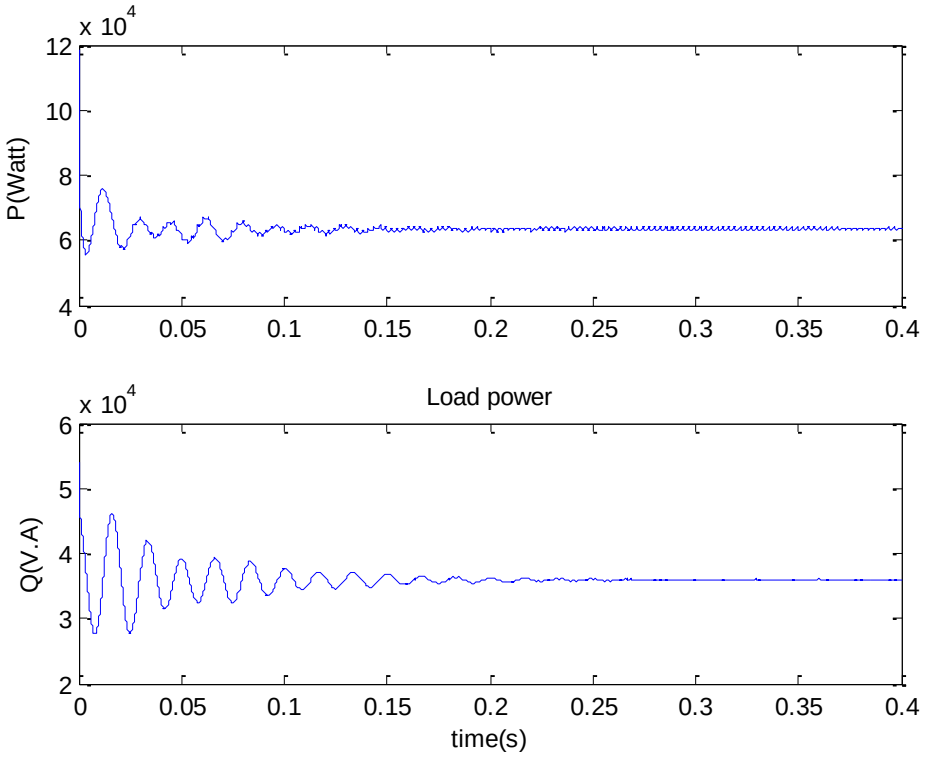

(a)

continued

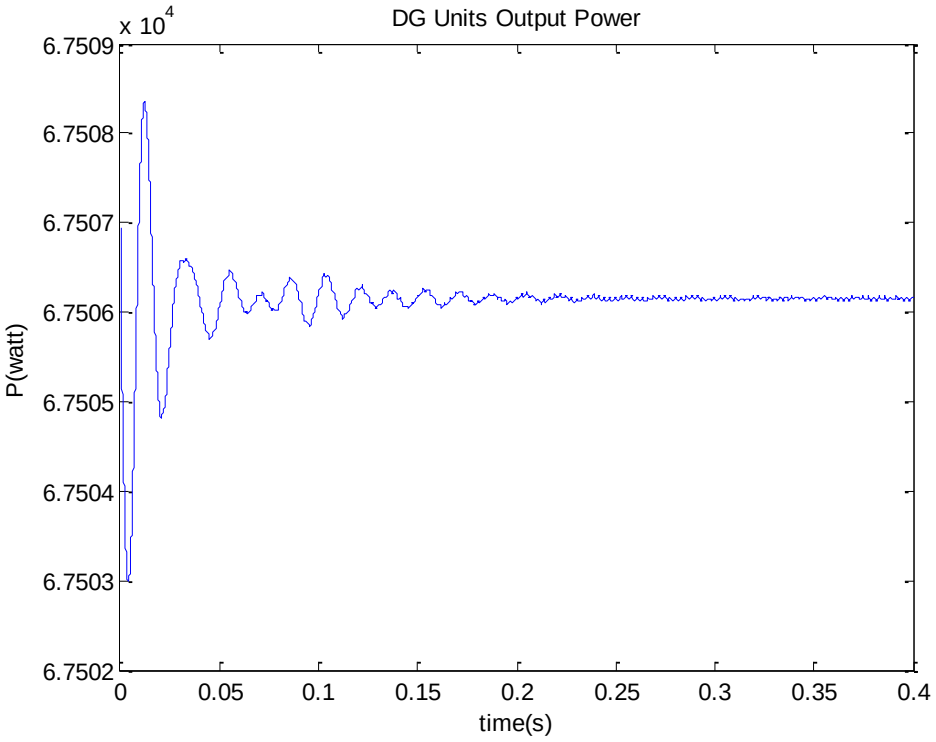

(b)

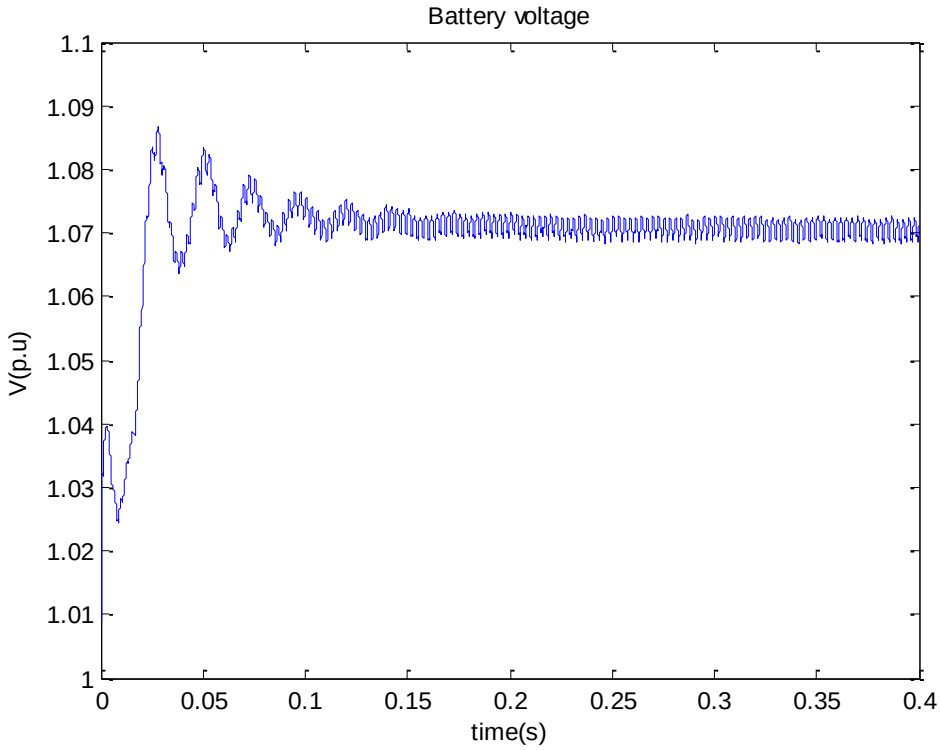

(c)

continued

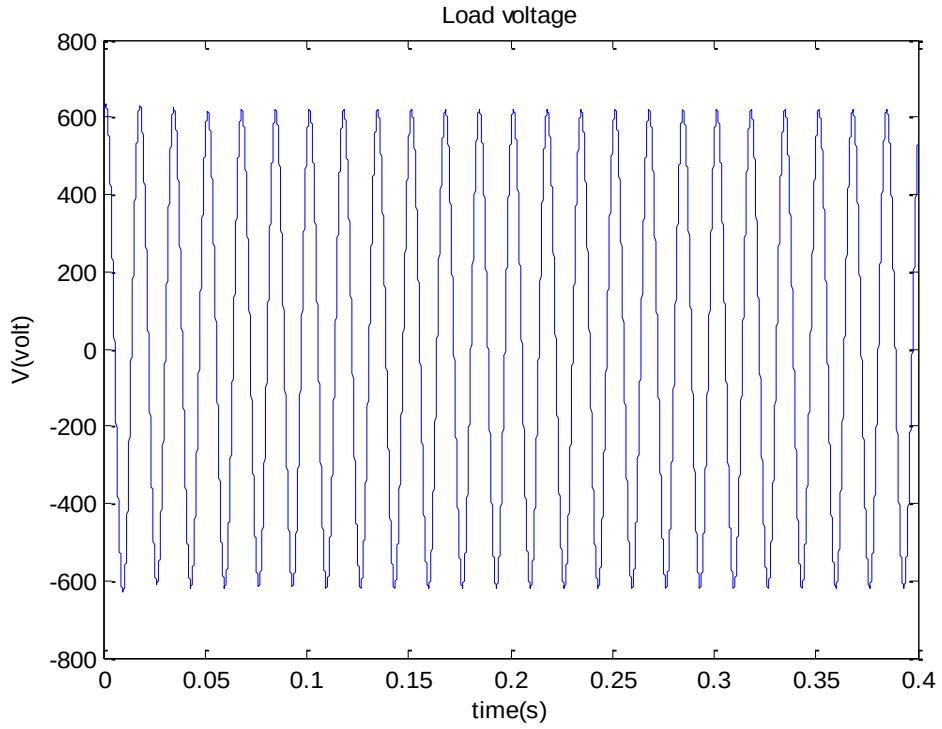

(d)

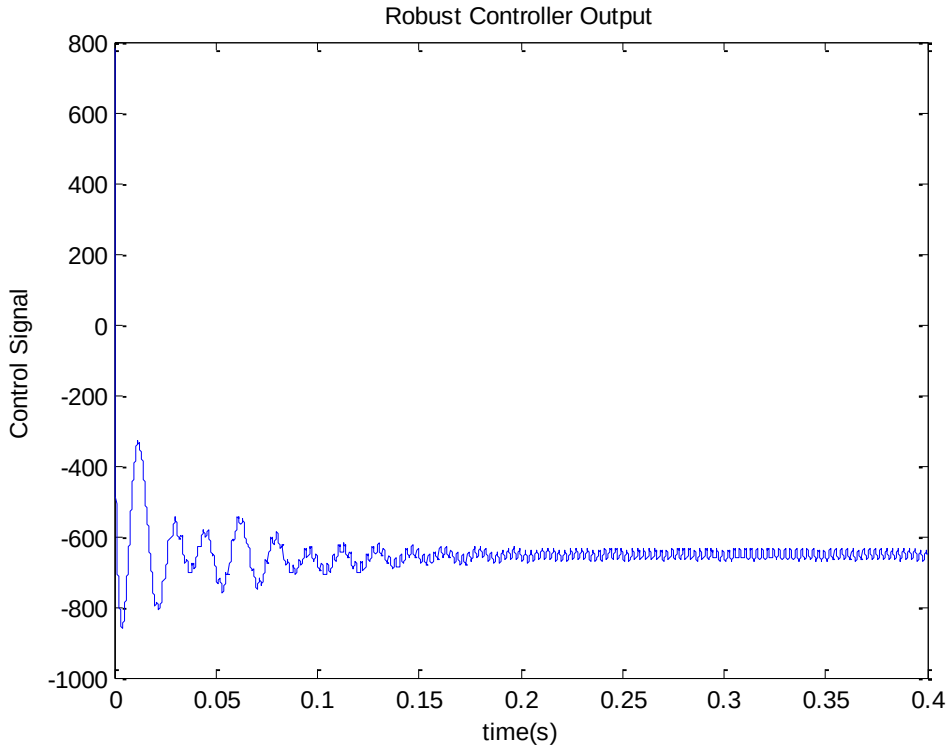

(e)

Fig. 4. For system charge mode: (a) Load Power; (b) DG's output power; (c) Battery DC voltage; (d) Load AC voltage; (e) Controller output.

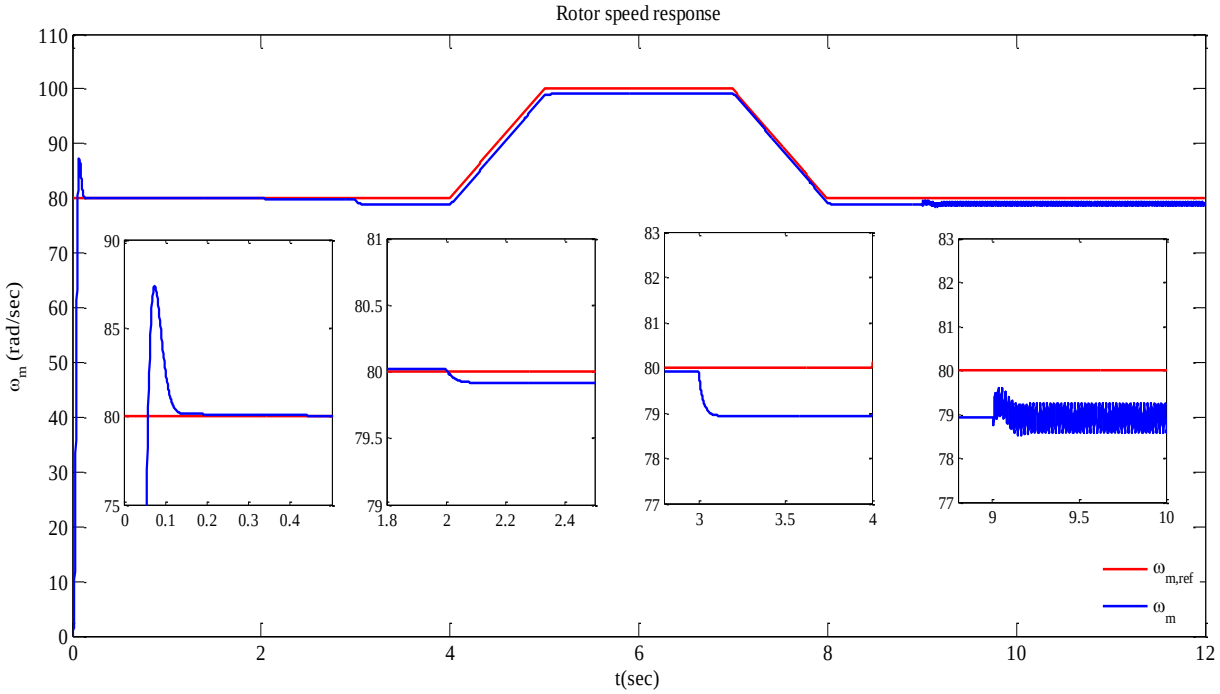

a) SMC with the conventional NBC.

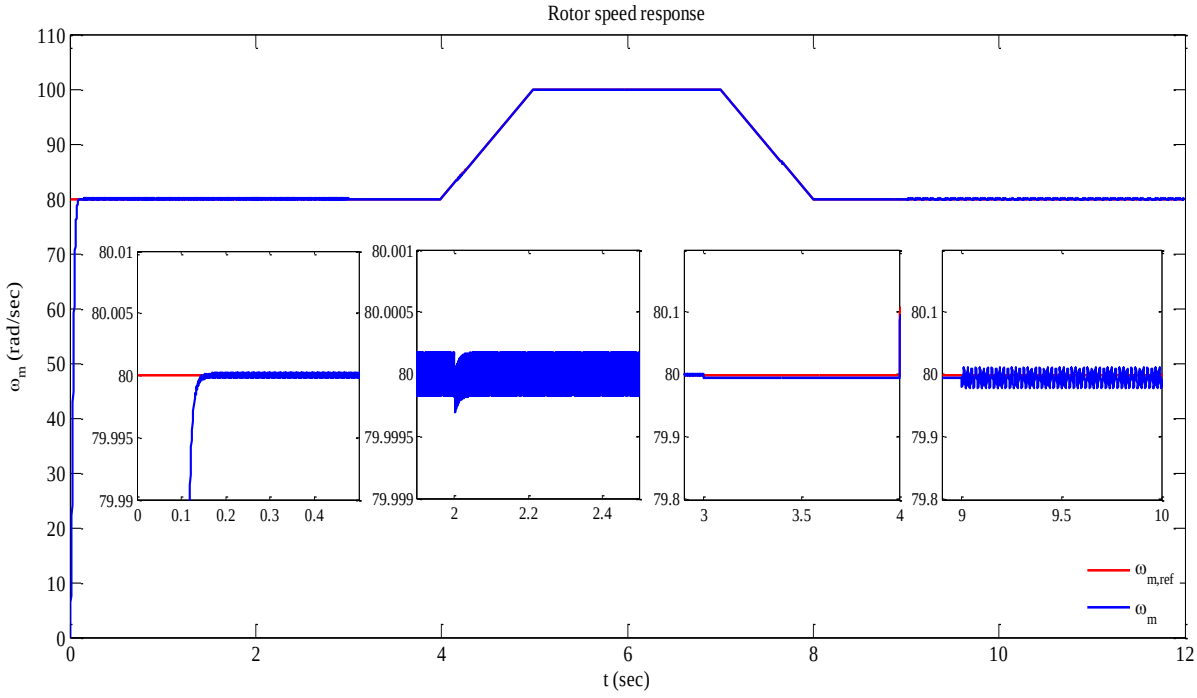

b) NSMC with the improved NBC.

Fig. 5. IM speed response.

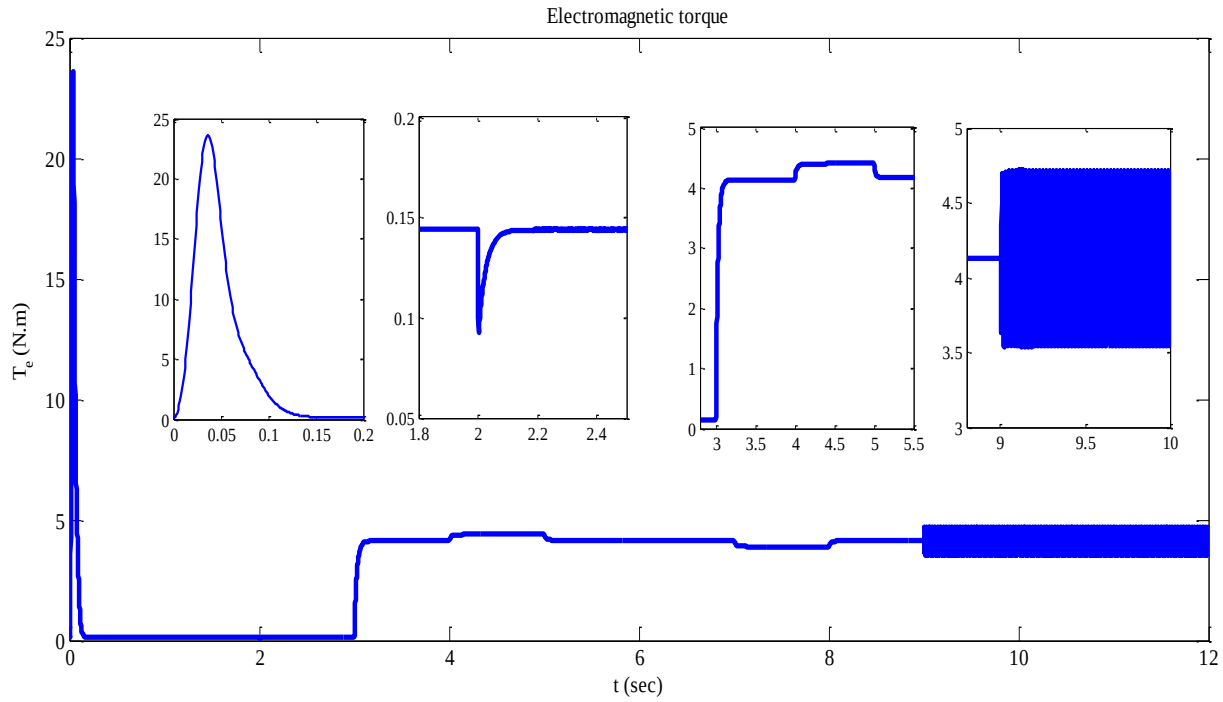

a) SMC with the conventional NBC.

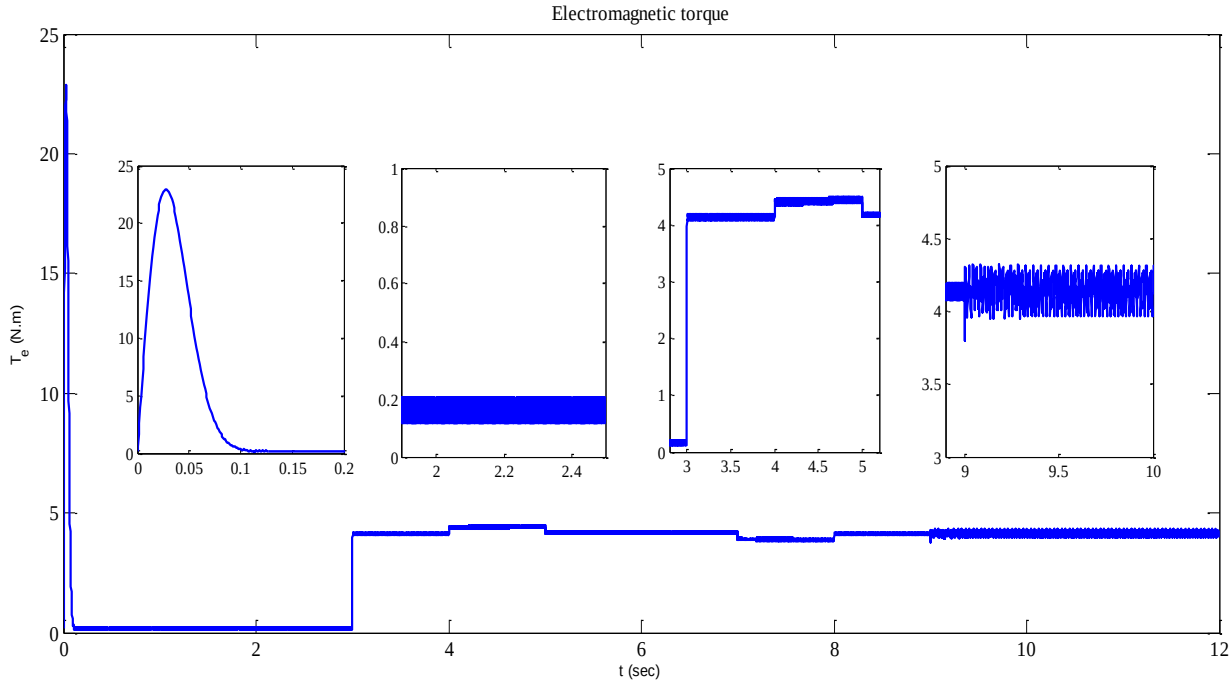

b) NSMC with the improved NBC.

Fig. 6: Electromagnetic torque.

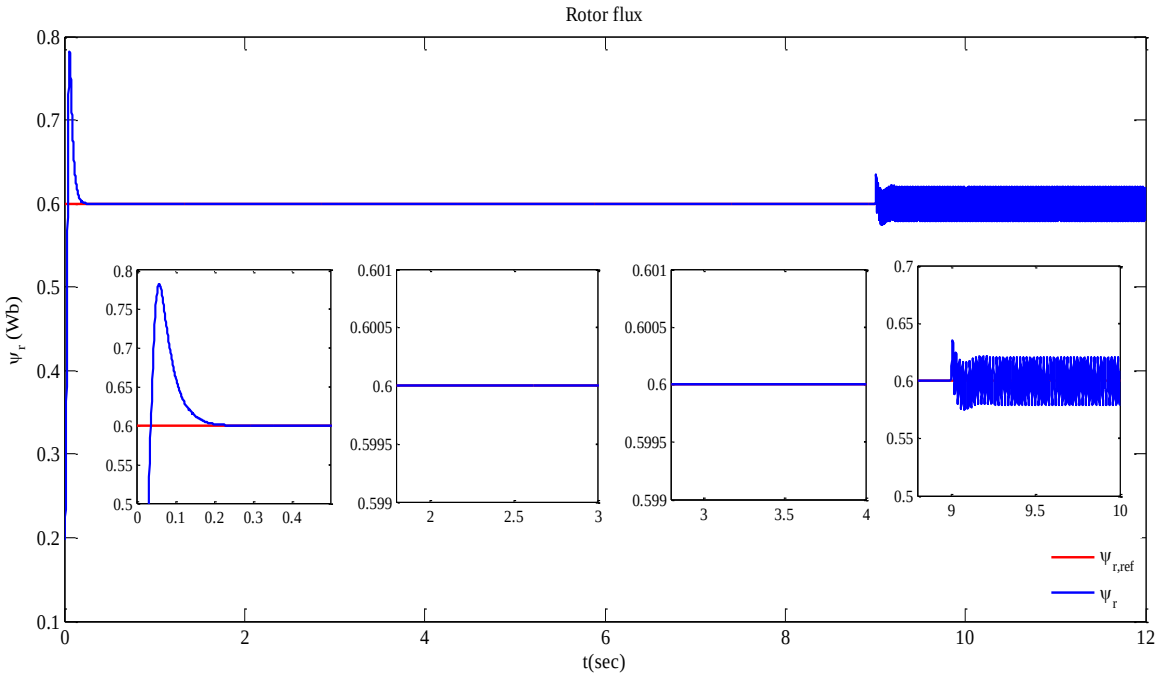

a) SMC with the conventional NBC.

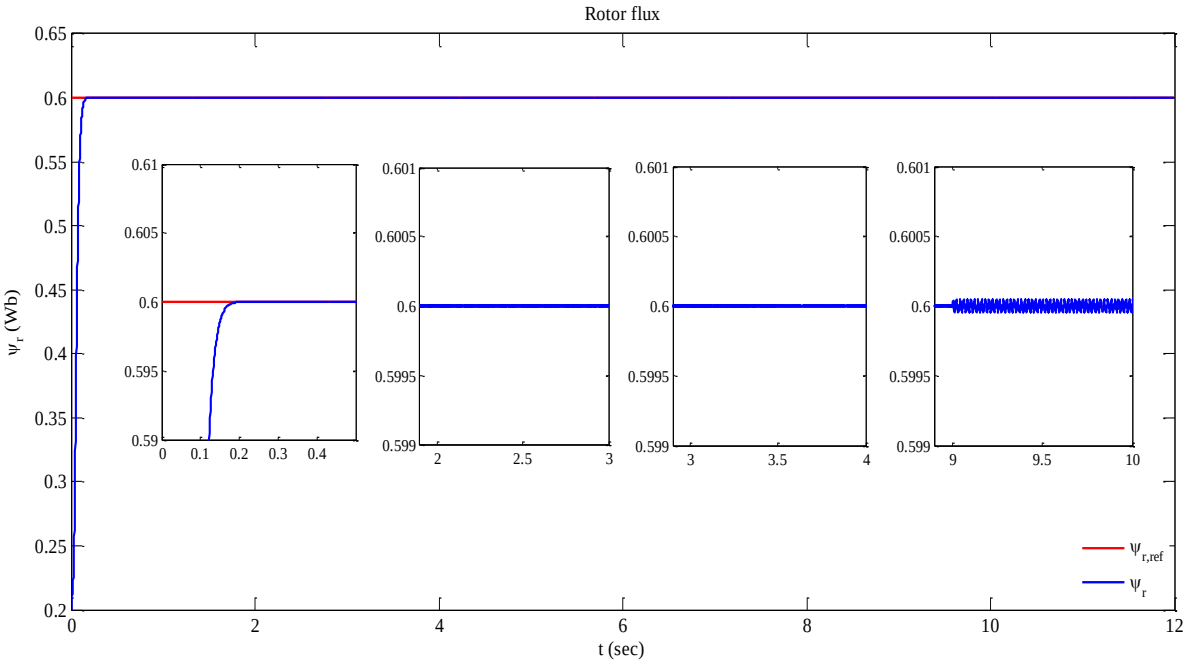

b) NSMC with the improved NBC.

Fig. 7. Rotor flux.

Comparative simulations of the discussed PFTC controllers (31) and (39) (SMC with the conventional NBC vs. NSMC with the improved NBC) are presented in Figures 5-10. The IM speed response, electromagnetic torque, rotor flux, stator currents, speed and flux tracking errors, and new transformation variables are shown in these figures.

The simulation test involves the following operating sequences:

- In order to examine the robustness of the proposed controllers regarding rotor faults, the IM responses with rotor resistance variation of $+100\%R_r$ is adapted. This resistance variation is considered in $t = 2s$.
- The motor shaft is subjected to a step load torque variation of $4Nm$ at $t = 3s$ which is considered to be unknown.

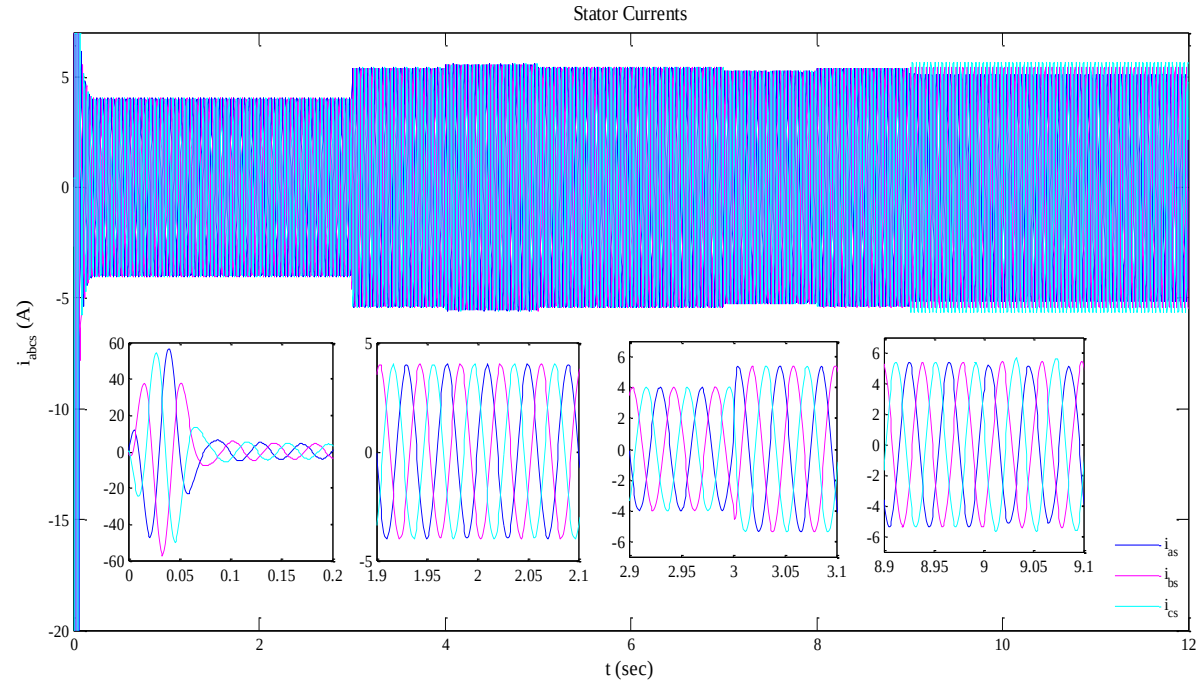

a) SMC with the conventional NBC.

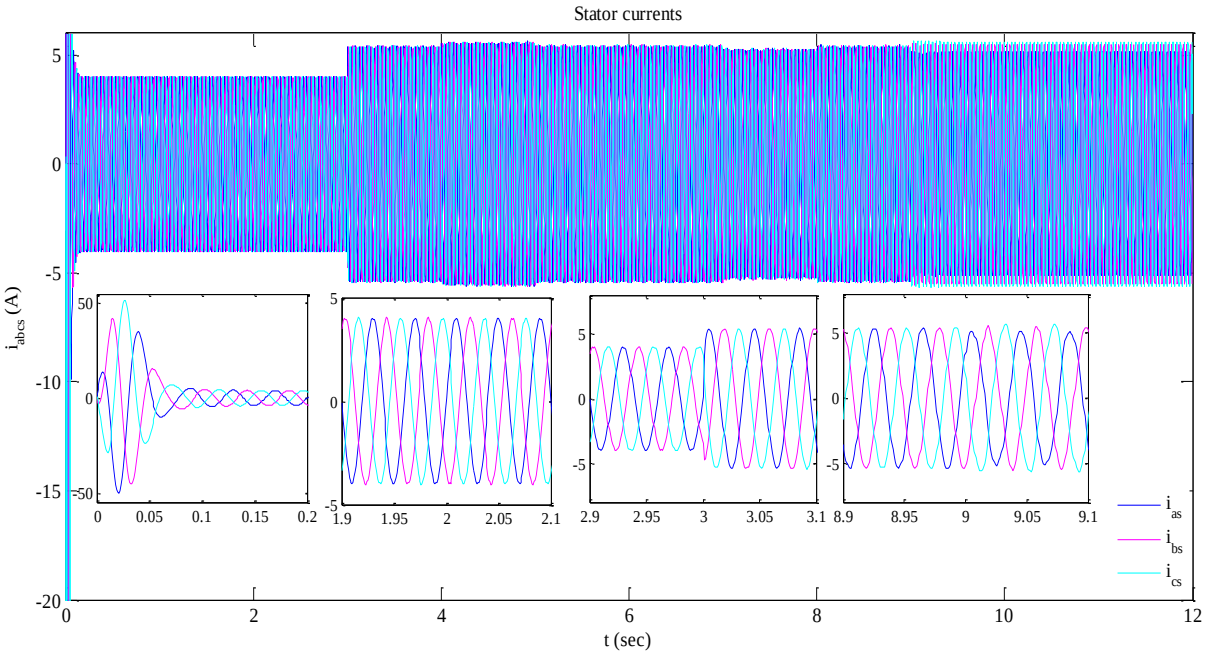

b) NSMC with the improved NBC.

Fig. 8. Stator currents.

- To investigate the proposed controller's performance under stator faults, simulations are carried out in the presence of static eccentricity. In order to simulate the fault of the stator, currents of the stator are destroyed by assuming that $A = 0.5$, $\varphi = 0$ and $\omega_c(t) + \theta_s(t)$ is computed using (6). Also, the time for stator fault occupancy is assumed in $t = 9s$.

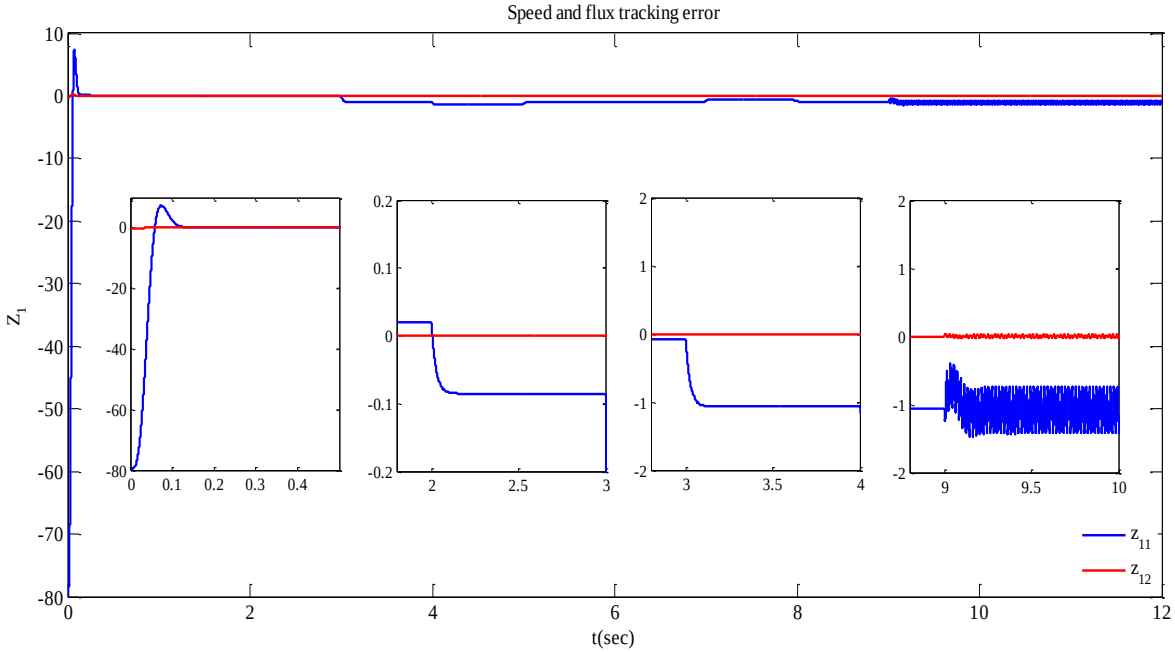

a) SMC with the conventional NBC.

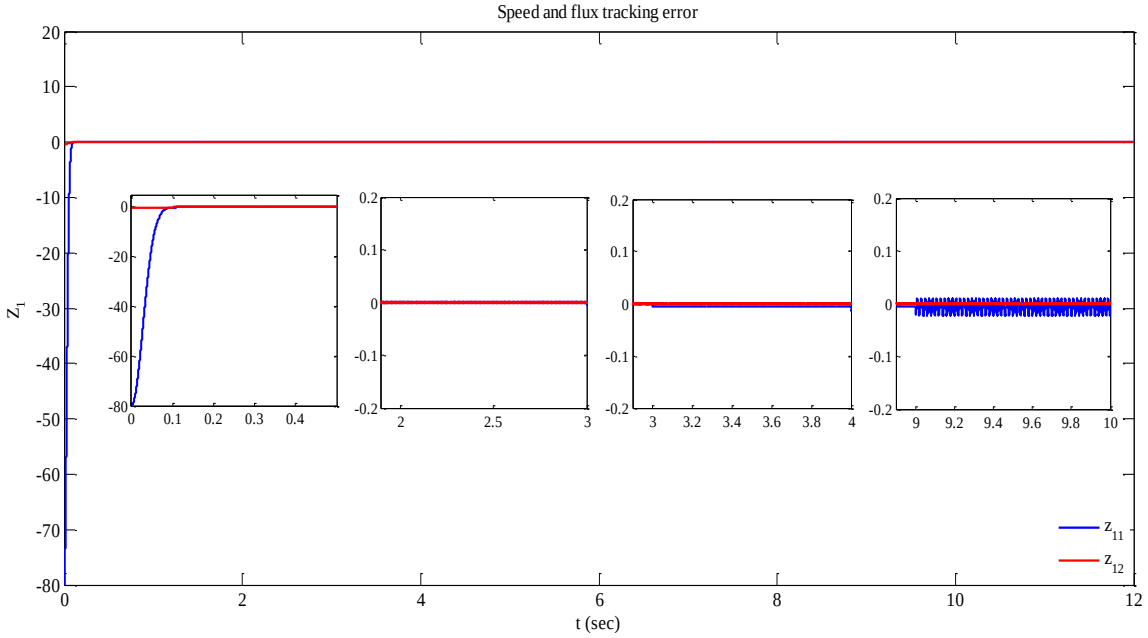

b) NSMC with the improved NBC.

Fig. 9. Speed and flux tracking errors.

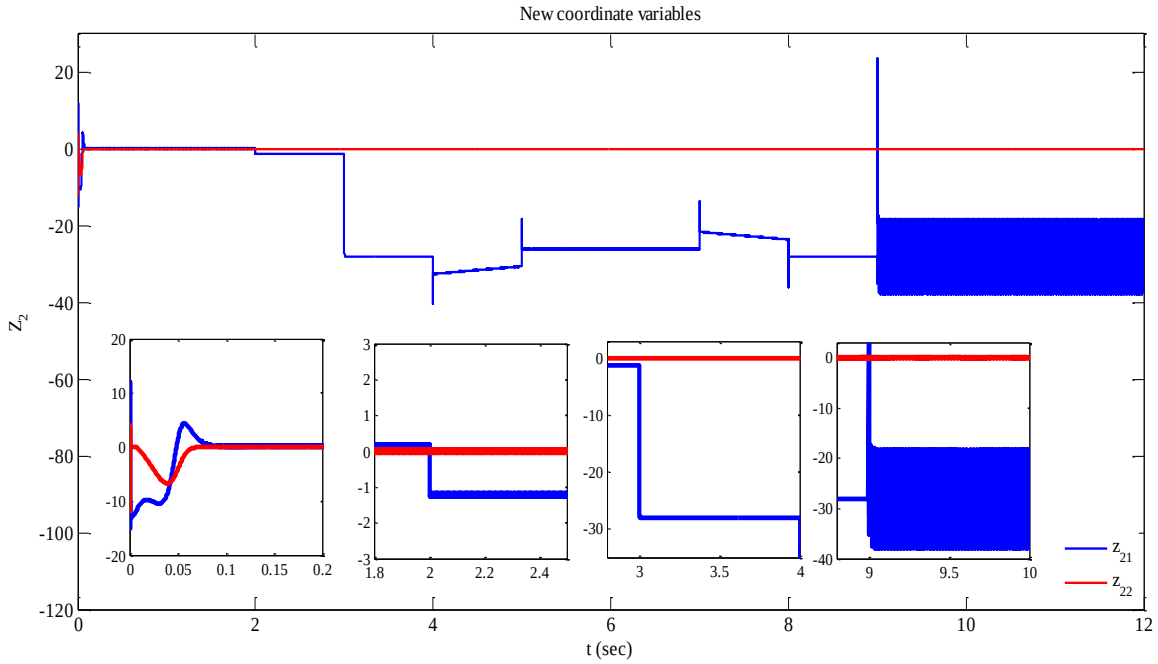

a) SMC with the conventional NBC.

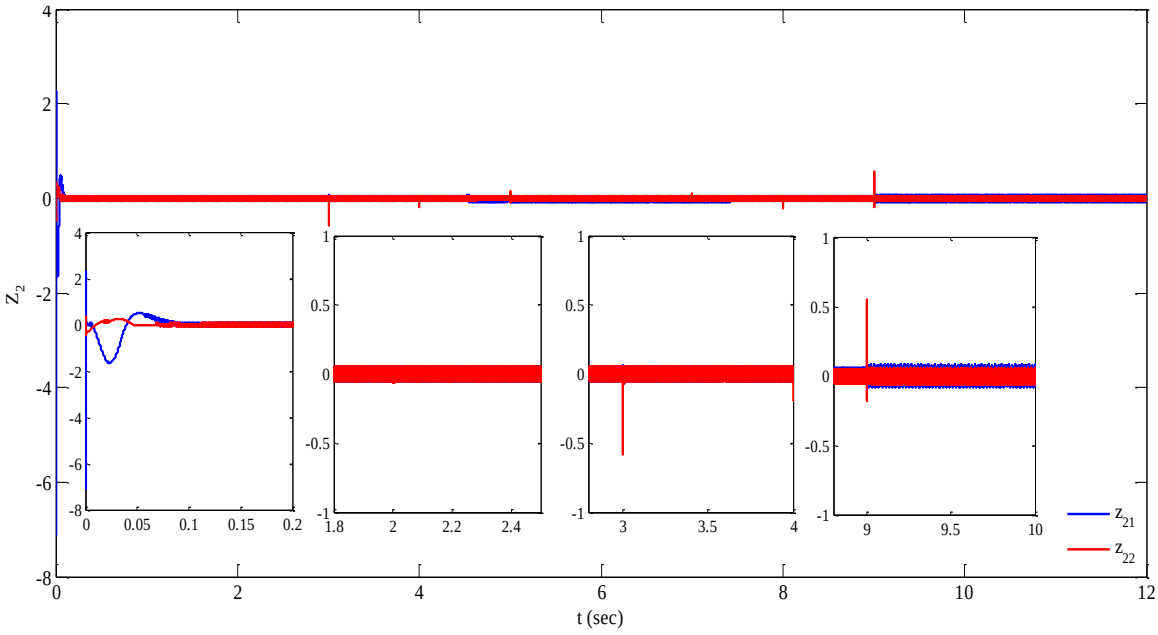

b) NSMC with the improved NBC.
Fig. 10. New coordinate variables.

Figures 5-10, demonstrate that the NSMC with the improved NBC technique has a low tracking error and low variation against different faults in comparison with the SMC with the conventional NBC approach. In addition, the unmatched fault effects are removed effectively. Furthermore, the NSMC with the improved NBC method

chattering is less than the SMC with the conventional NBC method.

7. CONCLUSION

Impact resistant H-infinity controllers on the inverter were connected to microgrids in this study. The role of H-infinity controller for controlling the micro-grid was as a filter. An undetermined value of the resistor, capacitor, and inductor filter was intended as a parameter. However, the micro-grid resistance was assumed with uncertainty. In order to reduce the overall computation time of the system, the designed controller for DG inverters employed a newly developed MPC algorithm which decomposed the control problem into transient sub-problems and steady state. The entire presented system was simulated using MATLAB/SIMULINK and then simulation results illustrated the effective performance of the proposed system. Micro-grids with renewable DGs such as solar cells and lithium-ion batteries that were connected to the network via converters were used as the reactive power compensation of nonlinear loads. In addition, a robust control method was used for controlling the inverter switches for batteries connected to the power network.

REFERENCES

[1] S. Braithwait, Behavior management, IEEE Power And Energy mag., vol. 8, no. 3, pp. 36–45, 2010.

[2] N. Jenkins, J. Ekanayake, and G. Strbac, Distributed Generation. London, U.K, 2009.

[3] A. Barbato, A. Dede and D. Giustina The potential for peak shaving on low voltage distribution networks using electricity storage, Journal of Energy Storage, vol. 16, pp. 231-242, 2018.

[4] G. Li, Parallel loop configuration for hybrid heat pump – gas fired water heater system with smart control strategy, Applied Thermal Engineering, vol. 138, pp. 807-818, 2021.

[5] A. Mondal and M. S. Illindala, "Improved Frequency Regulation in an Islanded Mixed Source Microgrid Through Coordinated Operation of DERs and Smart Loads," in IEEE Transactions on Industry Applications, vol. 54, no. 1, pp. 112-120, 2021.

[6] Hara S., Yamamoto Y., Omata T., Nakano M.: 'Repetitive Control System: A New Type Servo System For Periodic Exogenous Signals', IEEE Trans. Autom. Control, vol. 33, no. 7 Pp. 659–668, 1998.

[7] B. A. Francis, W. M. Wonham, "The Internal Model Principle for Linear Multivariable Regulators", Appl. Math. Optim, vol. 2, no. 2, pp. 170–194, 1998.

[8] Macana, Carlos A., et al. "A distributed real-time energy management system for inverter-based microgrids." Electric Power Systems Research 213 (2022): 108753.

[9] K. Jaesuk and S. Seung-Ki, "Harmonic currents control of three-phase four-wire grid-connected PWM inverter based on high-order repetitive controller," 2015 9th International Conference on Power Electronics and ECCE Asia (ICPE-ECCE Asia), pp. 2161-2166, 2018.

[10] Y. Wang, D. Wang, B. Zhang, K. Zhou,

‘Fractional Delay Based Repetitive Control with Application to PWM DC/AC Converters’. IEEE Int. Conf. On Control Applications, 2007.

[11] F. Xiao, L. Dong, L. Li and X. Liao, "A Novel Open-Loop Frequency Estimation Method for Single-Phase Grid Synchronization Under Distorted Conditions," in IEEE Journal of Emerging and Selected Topics in Power Electronics, vol. 5, no. 3, pp. 1287-1297, 2021.

[12] C. G. Dias and F. H. Pereira, "Broken Rotor Bars Detection in Induction Motors Running at Very Low Slip Using a Hall Effect Sensor," in IEEE Sensors Journal, vol. 18, no. 11, pp. 4602-4613, 2018.

[13] Y. Yu, Y. Zhao, B. Wang, X. Huang and D. Xu, "Current Sensor Fault Diagnosis and Tolerant Control for VSI-Based Induction Motor Drives," in IEEE Transactions on Power Electronics, vol. 33, no. 5, pp. 4238-4248, May 2019.

[14] X. B. Wang, Z. X. Yang and X. A. Yan, "Novel Particle Swarm Optimization-Based Variational Mode Decomposition Method for the Fault Diagnosis of Complex Rotating Machinery," in IEEE/ASME Transactions on Mechatronics, vol. 23, no. 1, pp. 68-79, 2018.

[15] M. E. H. Benbouzid, D. Diallo and M. Zeraoulia, Advanced Fault-Tolerant Control of Induction-Motor Drives For EV/HEV Traction Applications: From Conventional to Modern and Intelligent Control Techniques, IEEE Trans. Vehicular Technology, vol. 56, No. 2, Pp. 519-528, 2007.

[16] Y. Peng, W. Qiao, L. Qu and J. Wang, "Sensor Fault Detection and Isolation for a Wireless Sensor Network-Based Remote Wind Turbine Condition Monitoring System," in IEEE Transactions on Industry Applications, vol. 54, no. 2, pp. 1072-1079, 2021.

[17] T. A. Najafabadi, F. R. Salmasi and P. Jabehdar-Maralani, "Detection and Isolation of Speed-, DC-Link Voltage-, and Current-Sensor Faults Based on an Adaptive Observer in Induction-Motor Drives," in IEEE Transactions on Industrial Electronics, vol. 58, no. 5, pp. 1662-1672, 2011.

[18] K. S. Gaeid, H. W. Ping, M. Khalid and A. Masaoud, Sensor And Sensorless Fault Tolerant Control For Induction Motors Using Wavelet Index Sensors, Sensors, vol. 12, no. 4, pp. 4031-4050, 2021.

[19] Q. Gao, G. M. Asher and M. Sumner, "Implementation of sensorless control of induction machines using only fundamental PWM waveforms of a two-level converter," in IET Power Electronics, vol. 6, no. 8, pp. 1575-1582, 2013.

[20] M. Ghanes, J. P. Barbot, J. D. Leon and A. Glumineau, A Robust Sensorless Output Feedback Controller of the Induction Drives: New Design and Experimental Validation, International Journal of Control, vol. 83, no. 3, pp. 484-497, 2010.

[21] M. S. Zaky, M. K. Metwaly, H. Z. Azazi and S. A. Deraz, "A New Adaptive SMO for Speed Estimation of Sensorless Induction Motor Drives at

Zero and Very Low Frequencies," in IEEE Transactions on Industrial Electronics, vol. 65, no. 9, pp. 6901-6911, Sept. 2018.

[22] W. C. Andrade Pereira et al., "Improved Sensorless Vector Control of Induction motor Using Sliding Mode Observer," in IEEE Latin America Transactions, vol. 14, no. 7, pp. 3110-3116, 2021.

[23] N. Djeghali, M. Ghanes, S. Djennoune And J. Barbot, Sensorless Fault Tolerant Control for Induction Motors, International Journal of Control, Automation, And Systems, vol. 11, no. 3, pp. 563-576, 2019.

[24] A. G. Loukianov, Robust Block Decomposition Sliding Mode Control Design, Mathematical Problems in Engineering, vol. 8, pp. 349-365, 2002.

[25] A. Capozzoli, L. Celentano, C. Curcio, A. Liseno and S. Savarese, "Optimized Trajectory Tracking of a Class of Uncertain Systems Applied to Optimized Raster Scanning in Near-Field Measurements," in IEEE Access, vol. 6, pp. 8666-8681, 2022.

[26] Akpolat, Alper Nabi, Erkan Dursun, and Pierluigi Siano. "Inverter-based modeling and energy efficiency analysis of off-grid hybrid power system in distributed generation." Computers & Electrical Engineering 96 (2021): 107476.

[27] Meraj, Sheikh Tanzim, et al. "Energy management schemes, challenges and impacts of emerging inverter technology for renewable energy integration towards grid decarbonization." Journal of Cleaner Production (2023): 137002.

[28] D. Morinigo-Sotelo, R. J. Romero-Troncoso, J. A. Antonino-Daviu and K. N. Gyftakis, "Reliable detection of broken rotor bars in induction motors via MUSIC and ZSC methods," 2016 XXII International Conference on Electrical Machines (ICEM), Lausanne, pp. 2881-2886, 2016.